Sensitivity of the Numerical Prediction of Turbulent Combustion Dynamics in the LIMOUSINE Combustor

Mina Shahi
e-mail: m.shahi@utwente.nl

Jim B. W. Kok

Artur K. Pozarlik

J. C. Roman Casado

Laboratory of Thermal Engineering Enschede,
Faculty of Engineering Technology,
University of Twente,
Enschede 7500 AE, Netherlands

Thomas Sponfeldner
Department of Mechanical Engineering,
Imperial College London,
London SW7 2AZ, UK

The objective of this study is to investigate the sensitivity and accuracy of the reaction flow-field prediction for the LIMOUSINE combustor with regard to choices in computational mesh and turbulent combustion model. The LIMOUSINE combustor is a partially premixed, bluff body-stabilized natural gas combustor designed to operate at 40–80 kW and atmospheric pressure and used to study combustion instabilities. The transient simulation of a turbulent combusting flow with the purpose to study thermoacoustic instabilities is a very time-consuming process. For that reason, the meshing approach leading to accurate numerical prediction, known sensitivity, and minimized amount of mesh elements is important. Since the numerical dissipation (and dispersion) is highly dependent on, and affected by, the geometrical mesh quality, it is of high importance to control the mesh distribution and element size across the computational domain. Typically, the structural mesh topology allows using much fewer grid elements compared to the unstructured grid; however, an unstructured mesh is favorable for flows in complex geometries. To explore computational stability and accuracy, the numerical dissipation of the cold flow with mixing of fuel and air is studied first in the absence of the combustion process. Thereafter, the studies are extended to combustible flows using standard available ANSYS-CFX *combustion models. To validate the predicted variable fields of the combustor's transient reactive flows, the numerical results for dynamic pressure and temperature variations, resolved under structured and unstructured mesh conditions, are compared with experimental data. The obtained results show minor dependence on the used mesh in the velocity and pressure profiles of the investigated grids under nonreacting conditions. More significant differences are observed in the mixing behavior of air and fuel flows. Here, the numerical dissipation of the (unstructured) tetrahedral mesh topology is higher than in the case of the (structured) hexahedral mesh. For that reason, the combusting flow, resolved with the use of the hexahedral mesh, presents better agreement with experimental data and demands less computational effort. Finally, in the paper, the performance of the combustion model for reacting flow is presented and the main issues of the applied combustion modeling are reviewed.* [DOI: 10.1115/1.4025373]

Keywords: structured mesh, unstructured mesh, RANS solver, partially premixed combustion

Introduction

The first step for the computational fluid dynamics (CFD) calculation is the generation of a mesh in the domain of interest, on which the governing partial differential transport equations can be discretized. Nowadays, many different element and grid types are available; however, the choice highly depends on the problem and the solver capabilities, because every method has advantages and disadvantages. One category of meshes is the structured meshes. A structured mesh is a mesh that uses a uniform element shape. The topology of the cells in a structured mesh is specified for the mesh as a whole and is not deduced from the nodes. Another type of mesh is the unstructured mesh. Unlike a structured mesh, unstructured grids employ an irregular mesh to cover a volume, using geometry mesh entities, like faces, edges, and nodes [1,2]. An overview of unstructured mesh techniques for computational fluid dynamics is given by Mavriplis [3] and Kikuchi [4].

In general, structured grid approaches are often used with implicit formulations [5], while unstructured methods seem to be more conveniently used with the explicit formulations [6]. In general, implicit methods used on structured grids seem to be more stable, accurate, and converge faster, at least for a large class of practical test cases [7]. In this specific context, to the best knowledge of the authors, there is no literature directly evaluating the impact of using fully structured versus unstructured flow solvers on Reynolds-averaged Navier–Stokes (RANS) modeling of combustible flows.

Hansen and Forsythe [8] investigated the performance of unstructured grids for turbulence resolving calculations in the application of flow over a circular cylinder at Reynolds numbers 3900–140,000. They came to the conclusion that good comparison with experimental data was obtained with the use of structured grids for variables like the Strouhal number, time-averaged drag, back pressure, and recirculation zone length. For simulations of flows at a Reynolds number of 140,000, the time-averaged coefficient of pressure and drag fell within two separate sets of experiments and closely match a similar set of computations on structured grids using a high order of discretization solver.

Studies done by Hua et al. [9] on the flow near a spur dike indicate that the precision with unstructured grids is higher than that

Contributed by the Combustion and Fuels Committee of ASME for publication in the Journal of Engineering for Gas Turbines and Power. Manuscript received July 15, 2013; final manuscript received August 12, 2013; published online October 28, 2013. Editor: David Wisler.

with structured grids despite that the central processing unit time required is slightly more with unstructured grids.

Studies done by Tomita et al. [10] showed the strong influence of mesh type on the flow quantities. However, they proved that, for both structured and unstructured mesh types, the shear stress transport (SST) turbulence model presented good prediction compared to experiments, while for simulations with other turbulence models, like Reynolds stress model, results using the structured mesh were superior.

Hence, it can be concluded that, on the basis of the literature, the accuracy of the flow simulation is sometimes, but not always, best with a structured solver, and it seems to be dependent on the flow geometry and the quality of the mesh generator. For this reason, our purpose in this study is to explore the performance and limitations of certain structured and unstructured grids to investigate the numerical dissipation of the fuel/air mixture flow, specifically for the bluff body flow in the LIMOUSINE combustor. The experimental configuration and computational domain are first introduced in the section Combustor Setup. The next section, Numerical Method, provides the details about the numerical methods, meshes, and sets of boundary conditions used for CFD calculations. The applied physical models for turbulence and combustion are presented in the section Modeling of Turbulence and Combustion. Due to the importance of the mixing as a determining factor in the combustion modeling, the first part of the Results section is devoted to the analysis of the mixture flow in the absence of the combustion process. CFD predictions obtained by using a fully structured and a fully unstructured solver are discussed and compared to experiments. Subsequently, studies are extended to flows with combustion using the combustion models standard available in ANSYS-CFX.

Combustor Setup

The experiment, which is used as a basis for modeling studies, is performed on a test rig that is shown in Fig. 1. It is located at the University of Twente and four other laboratories, within the framework of the European Marie Curie Initial Training Network project "LIMOUSINE" (see Appendix A). The setup is designed to study limit cycles of combustion rate oscillations due to thermoacoustic instability. The combustor consists of two sequentially coupled rectangular ducts with different widths, with the burner in between the two ducts. The duct upstream of the burner has a $25 \times 150\ \text{mm}^2$ cross section and is 275 mm long, whereas the duct downstream of the burner has a cross-sectional area enlarged to $50 \times 150\ \text{mm}^2$ to partly compensate the volume expansion due to the combustion. In the transition between the ducts, the burner is mounted, which creates a flow recirculation pattern that stabilizes the flame by means of a triangular bluff body. In this configuration, which is the third design version of the combustor (V3), the total length of the combustor is 1050 mm (see Table 1 for dimensions). Therefore, the width (150 mm) of the combustor is much larger than the depth (50 mm) but much less than the height and the system approximates, in behavior, a two-dimensional combustor. Details about dimensions of the model combustor are summarized in Table 1. Air as the oxidizer is injected at the upstream end. The flow recirculation that stabilizes the flame is, in this case, created by a wedge, which is placed at the point where the small duct is attached to the large duct. From the side surfaces of the wedge, gaseous fuel is injected through 62 holes. The fuel used here is methane at room temperature. All pieces, except the brass bluff body, are made from heat-resistant stainless steel S310. The only cooling of the combustor is by natural convection

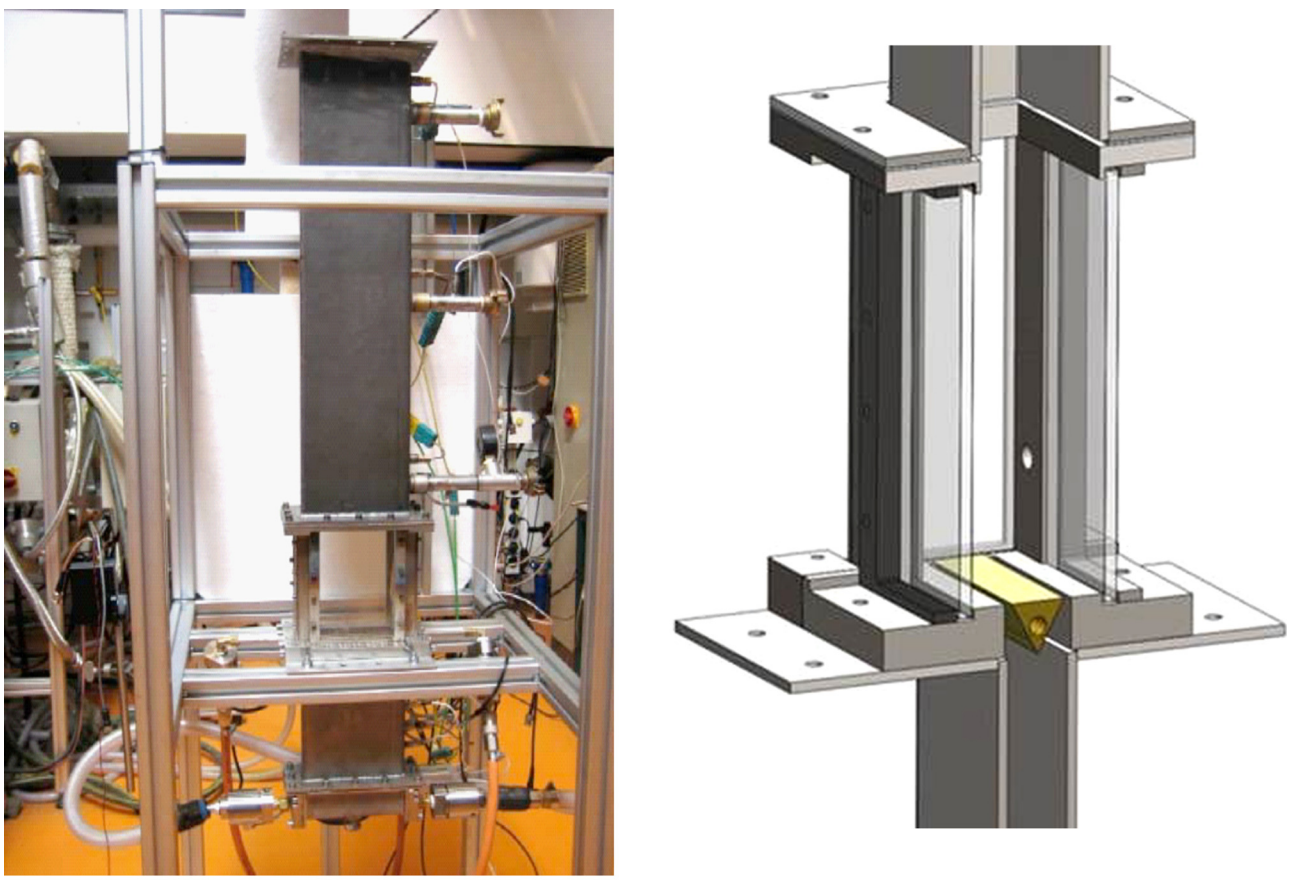

(a) (b)

Fig. 1 (*a*) Experimental setup; (*b*) LIMOUSINE burner

Table 1 Dimensions of the model combustor

Location	Dimension (mm)
Upstream height	220
Upstream width	25
Downstream height	780
Downstream width	50
Width of the combustor in the third direction	150

and radiation at the outside surfaces. The burner can operate at a range of power of 20–80 kW and air factor 0.8–2.

This configuration behaves like a variation of a Rijke tube [11] but with forced inlet air flow and closed acoustic upstream condition.

Numerical Method

The CFD code employed here is ANSYS-CFX 14.0. It uses an implicit finite volume formulation to construct the discretized equations representing the Reynolds-averaged Navier–Stokes equations for the fluid flow. The model consists of a compressible solver with a colocated (nonstaggered) finite volume method, such that the control volumes are identical for all transport equations [12]. To avoid the decoupling of the pressure field, CFX uses the Rhie–Chow [13] discretization method for the mass terms, as modified by Majumdar [14]. A coupled algebraic multigrid solver is used to give robust solutions for the governing system of linearized equations representing the differential transport equations in discretized form. For the discretization of the governing equations, a high resolution advection scheme spatial method and a second order backward Euler discretization for time accuracy is used. The computational geometry used in the solution process is illustrated in Fig. 2

Details about boundary conditions imposed on the domain are summarized in Table 2. The flow parameters are set consistent with the experimental conditions depicted in Table 3. The closed acoustic inlet boundary condition at the upstream end was implemented by prescribing a uniform and steady inlet velocity profile at the air inlet, which ensured an acoustically closed inlet. The mass flow rate of fuel per unit cross-sectional area was specified at the fuel inlet. At the combustor outlet, the pressure was set to a constant value of 1 atm, which represents the open acoustic boundary condition. In order to take into account the effect of heat losses through the walls, the walls were treated as convective boundaries, where an outside heat transfer coefficient and outside temperature were specified.

In this work, the effects of turbulence are simulated by using the SST turbulence model in the steady state calculations, while for the transient calculations, the scale-adaptive simulation model (SAS) is used. Reacting flow simulations are carried out on the model combustor using different combustion models, which are standard available in ANSYS-CFX. In the following sections, the used turbulence and combustion models are described briefly.

Modeling of Turbulence and Combustion

The SST Turbulence Model. The $k-\varepsilon$ turbulence model has two main weaknesses: overpredicting the shear stress in adverse pressure gradient flows due to too low dissipation and requirement for wall modification. The $k-\omega$ model is better in predicting the adverse pressure gradient flow, and it does not use any damping functions. However, it is dependent on the value of ω in the free stream flow. In order to improve these models, the SST model suggested by Menter [15] was developed. The SST is an eddy-viscosity model that uses a combination of $k-\varepsilon$ and $k-\omega$ models for the core flow and boundary layer, respectively. For this, a blending function F1 is introduced that is equal to one in the near wall region and equal to zero for the flow domain in the outer region. It smoothly switches from the $k-\omega$ model in the near wall region to the $k-\varepsilon$ model for the rest of the flow. In this way, the near wall performance of the k $-$ ω model can be used without the potential errors resulting from the free stream sensitivity of that model.

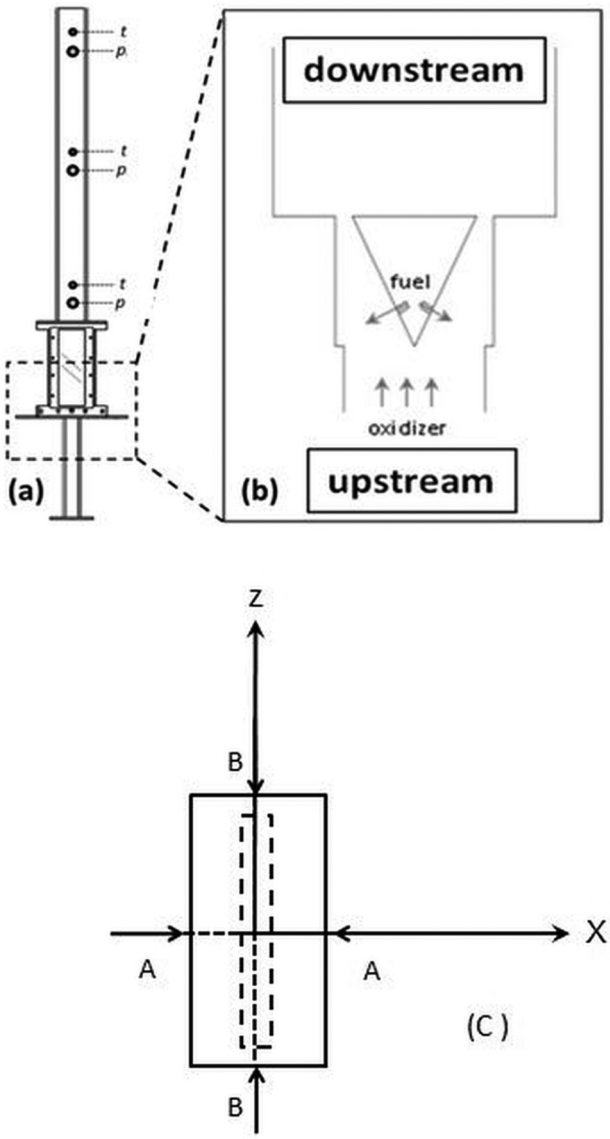

Fig. 2 A schematic representation of the model combustor: (*a*) computational domain in CFD calculation; (*b*) an enlarged view around the wedge; (*c*) cross-sectional area of the combustor (view from the top)

Table 2 Details about boundary condition

Location	Boundary condition
Air inlet	Normal speed
Fuel inlet	Mass flow rate
Outlet	Average static pressure
Walls	Nonslip

Table 3 Operating condition

Power (kW)	Air factor	Fuel mass flow rate (g/s)	Air mass flow rate (g/s)
40	1.4	0.8	19.152
60	1.2	1.2	24.624

Table 4 Number of elements for each mesh

	Structured mesh	Unstructured mesh
Number of elements	4,000,822	6,200,000

The SAS Turbulence Model. The scale-adaptive simulation (SAS) is an advanced unsteady RANS model that allows better resolution of the turbulence spectrum in unstable flow conditions. This model can change smoothly between large eddy simulation (LES)-like behavior in regions where the turbulence structure is well resolved and the SST model, where the unsteady flow is not well resolved. The starting point of the transformation to the SST model is the k-νt formulation, as given by Menter and Egorov [16].

Modeling of the Combustion. The simulations here have been carried out with the help of four different combustion models (available in ANSYS-CFX code), depending on suitability in terms of time and available computer capacity. Their basic principles and features are discussed in Appendix B.

Results and Discussions

Part I: Meshing Effects. All the meshes used in this study were generated using the meshing tool ANSYS WORKBENCH 14.0. Since the CFX solver uses the nodes to create control volumes around it, the number of nodes should be chosen as a congruence parameter. The grid that represents the flow domain can be unstructured (composed of hexahedra, tetrahedral, wedges, and pyramid control volume shapes) or structured. In general, structured meshes offer easy data access, while unstructured meshes offer more convenient mesh adaptivity and better fit to complex geometries. The big advantage of using the structured hexa meshes applications is that one can align the mesh relatively nicely with the flow direction, therefore reducing numerical diffusion and aiding convergence, and fewer elements are demanded to fill the considered domain. However, it should be noticed that, in each approach, the mesh adjacent to the wall should be fine enough to resolve the boundary layer flow. In boundary layers, quadrilateral, hexahedron, and prism/wedge cells are preferred over triangles, tetrahedrons, or pyramids.

Considering that all important turbulent structures and stresses are generated close to the wall, it is very important to control the distance of the first element from the wall surface, because different turbulence models have different requirements for mesh treatments to guarantee accurate results. For the unstructured mesh, it is possible to define the smaller and larger element sizes to control this distance from the wall surface. For the structured mesh generation, the control of the elements' distribution near the wall is more robust and the smoothing process as well as the use of different functions are possible. Since the resolution of the grid has significant effects on the accuracy of results, in this work, each mesh type was used for three different mesh sizes in each structured and unstructured approach, and the final mesh chosen for simulation is shown in Table 4. Figure 3 demonstrates the influence of the number of elements in the present configuration based on the vertical component of velocity profile at three different lines along the height of the combustor for structured and unstructured meshes. The velocity profiles on the final chosen grids are compared for three different lines taken from two different planes: plane A-A at midspan ($z=0$) and plane B-B at midpitch ($x=0$), which are respectively shown in Figs. 4 and 5. As it is obvious, in the plane ($z=0$), the unstructured grid predicts higher value of velocity in each location, while in the second plane ($x=0$) (see Fig. 5), smaller value is predicted by this grid, which points to the fact that the mass flow rate remains the same using any type of grid.

Mechanisms of Mixing. In the Reynolds-averaged approach, a model for the turbulent mass flux, $\langle u_j', c' \rangle$, is required to calculate averaged scalar fields, where u_j' and c' are fluctuating components of instantaneous velocity and instantaneous concentration of species, respectively. The gradient diffusion model [17] can be used to model $\langle u_j', c' \rangle$ given by

$$\langle \boldsymbol{u}_j', \boldsymbol{c}' \rangle = -\boldsymbol{K}_{jj} \frac{\partial(\boldsymbol{c})}{\partial \boldsymbol{x}_j}$$

where K_{jj} is the eddy diffusivity of the scalar concentration and is generally calculated from $K_{jj} = \vartheta_t / Sc_t$. ϑ_t stands for the turbulent viscosity obtained from another turbulent model, and Sc_t is a turbulent Schmidt number.

By ignoring reactions, sources, and molecular diffusion, similarly to molecular models, the following transport equation must be satisfied:

$$\frac{\partial \boldsymbol{c}_i}{\partial \boldsymbol{t}} + \bar{\boldsymbol{u}}_j \frac{\partial(\boldsymbol{c})}{\partial \boldsymbol{x}_j} = \frac{\partial}{\partial \boldsymbol{x}_j} \left(\boldsymbol{K}_{jj} \frac{\partial(\boldsymbol{c})}{\partial \boldsymbol{x}_j} \right)$$

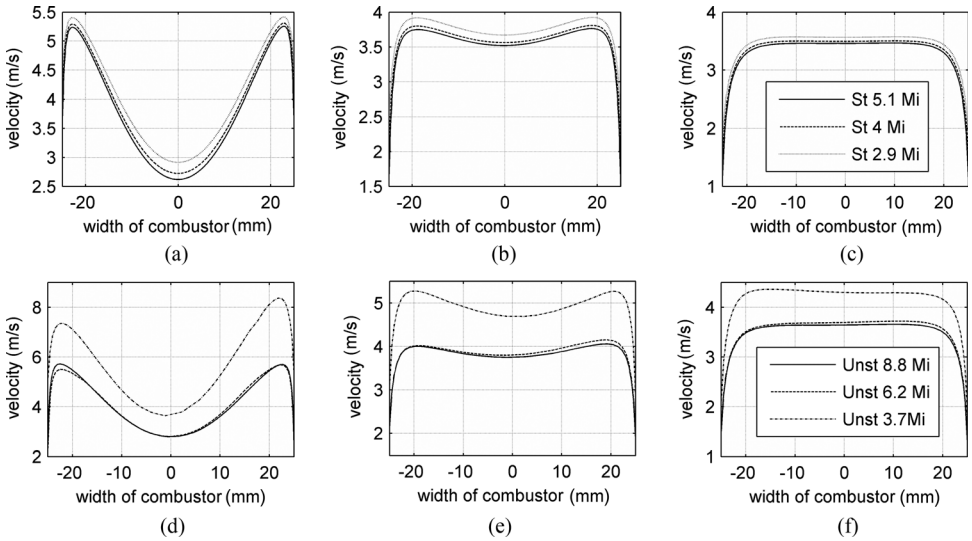

Fig. 3 Mesh-dependency studies of structured grid (st) at different locations: (*a*) $y=10$ cm, (*b*) $y=20$ cm, (*c*) $y=30$ cm and unstructured mesh (unst): (*d*) $y=10$ cm, (*e*) $y=20$ cm, (*f*) $y=30$ cm based on the streamwise velocity

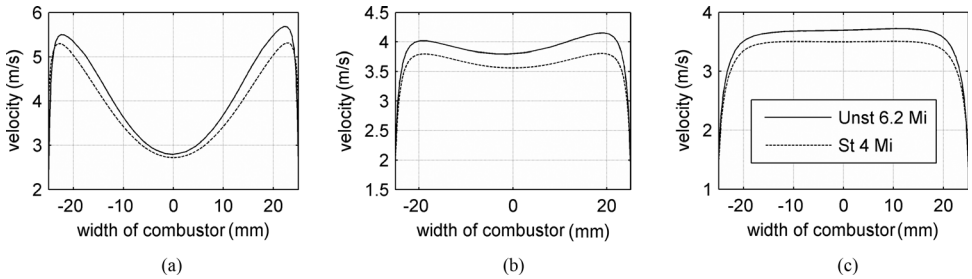

Fig. 4 Comparison of streamwise velocity for the chosen grids taken from cross section A-A at: (*a*) $y = 10$ cm, (*b*) $y = 20$ cm, (*c*) $y = 30$ cm

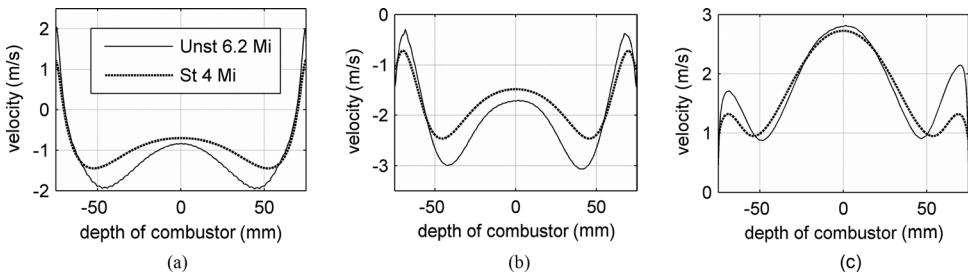

Fig. 5 Comparison of streamwise velocity for the chosen grids taken from cross section B-B at: (*a*) $y = 0.5$ cm, (*b*) $y = 10$ cm, (*c*) $y = 20$ cm

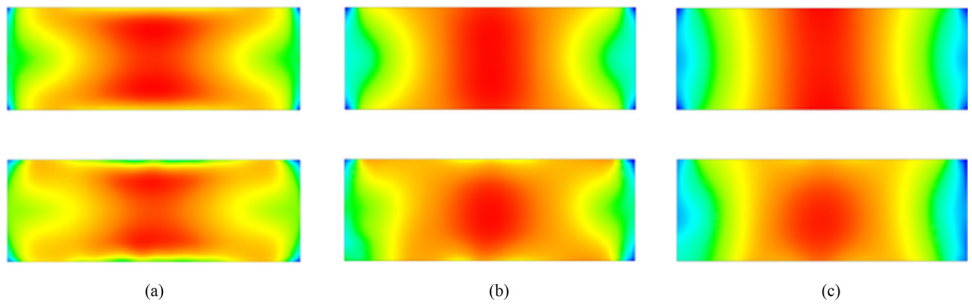

Fig. 6 Comparison of structured (st) (on top) and unstructured mesh (unst) (on bottom) on the mixing behavior of CH4 concentration at: (*a*) $y = 10$ cm, (*b*) $y = 20$ cm, (*c*) $y = 30$ cm

The eddy diffusivity is a matrix expression that may vary in space.

In this study, we measure the CH_4 concentration as well as the eddy viscosity in the absence of chemical reaction to investigate the effect of the chosen mesh on the gradient diffusion model. Figure 6 represents the effect of the chosen grid on the mixing behavior. The CH_4 mass concentration obtained by using each grid type is shown in three different cross-sectional planes along the height of the combustor. It can be assumed that, in this combustor, turbulent diffusion is several orders of magnitude larger than molecular diffusion, and therefore, ideally, prediction of turbulent mixing should not be affected by numerical diffusion [18]. However, much stronger mixing is predicted by the unstructured mesh, probably because of the strong numerical diffusion inherent to these grids (numerical artifact resulting from the use of a first-order upwind for discretizing the convection terms). Indeed, in the structured mesh, cells are aligned with the general flow direction giving lower numerical dissipation and lower cell count.

The obtained mixing results in the unstructured grid as well as the velocity profile presented in Fig. 3 are slightly asymmetric with respect to the center, which is not expected from a physical point of view.

Figure 7 shows the calculated turbulent eddy viscosity on two different types of grids. Although higher rate of mixing and therefore smaller gradient of concentration was predicted by the unstructured grid, the turbulent eddy viscosity and therefore the eddy diffusion is less in this case, confirming the existence of higher numerical diffusion attached to this grid, which leads to higher mixing. Overall, these results not only show how numerical diffusion affects the distribution of species, they also demonstrate how numerical diffusion can cause an unphysical asymmetric velocity profile.

Flow Characteristics. Figure 8 shows a time-averaged transient solution of the vertical velocity component, v, in the cold flow simulation as well as velocity measurements obtained with the particle image velocimetry (PIV) method averaged over 100 images, measured at Imperial College London. In each part of this figure, isocontours of $v = 0$ are shown, which represent the location of the recirculation zones (labeled with 0). Recirculation occurs in three regions: in the central recirculation zone (referred to as CRZ), which is stabilizing the flame, and also in two regions between the fresh fuel gas jets and near the liner of the downstream duct, referred to as outer recirculation zone.

The predictions compare quite well with the measurements in the center and outer recirculation regions, while the velocity magnitude in profiles close to the wall is overpredicted, especially in the case of using the unstructured grid. This can be due to the near

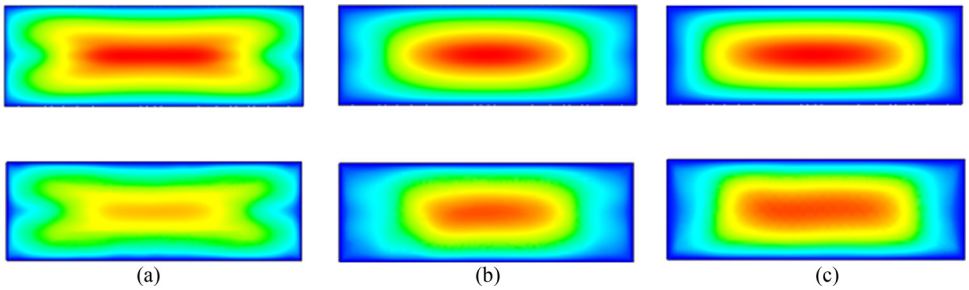

Fig. 7 Comparison of turbulent eddy viscosity calculated by structured (st) (on top) and unstructured mesh (unst) (on bottom) at (*a*) $y = 10$ cm, (*b*) $y = 20$ cm, (*c*) $y = 30$ cm

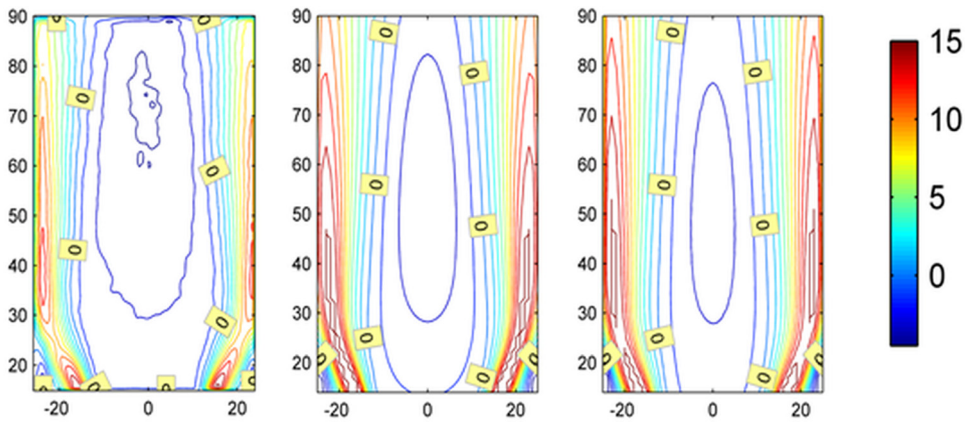

Fig. 8 Streamwise velocity component for 40 kW thermal power and air factor 1.4: experiment (left), structured mesh (middle), unstructured mesh (right)

wall treatment used in the simulations and the resulting cell size very close to the wall. A second explanation is that, in measurements very close to the walls, reflections from the laser beam tend to underpredict the velocity, due to bright spots or deposition of particles, etc. And lastly, at downstream positions of around 25 mm, the PIV data shows a region of lower velocities. This is due to reflections from the rear window causing underpredictions of the velocity similar to the regions close to the side walls. Furthermore, the core of the CRZ is more squeezed compared to measured data. However, the current predictions are able to capture the essential characteristics of the flow (i.e., stagnation points, etc.). Although there are some differences between simulations and experiments, the predicted pressure fluctuations, which will be discussed later, show very good agreement with experimental data.

Figure 9 shows the average velocity profiles on the chosen grids taken from the plane B-B (see Fig. 2) at midpitch ($x = 0$) across the entire stream and span. Calculations done on the structured grid show more uniform velocity profile in the streamwise direction compared to the unstructured grid, confirming the prediction of higher turbulent eddy viscosity in the structured mesh, as presented in Fig. 7. Considering the fact that the first and the last fuel injectors on the side surfaces of the wedge are far from the side walls in the spanwise direction (z), the presence of two corner recirculating zones (CORZ) is expected. These CORZs can squeeze the main flow and create a big recirculation zone in the middle, acting like a blockage where the flow expands around it. Under reacting conditions, this effect of blockage on the spanwise direction should be less because of higher acceleration of flow and thermal expansion. However, due to the tendency of hot spices and products to rise (according to a chimney effect), still this blockage may emerge (see Fig. 10).

Figures 11 and 12 show the enlarged view of the mesh around the wedge for the structured and unstructured grids, respectively. Due to having very small scales in the geometry (i.e., 1-mm fuel holes and 3-mm burner passage slots), generating a mesh with good quality and without massive jumps in the element size or introducing high aspect ratios is very difficult. Despite these difficult aspects of the combustor design, care was taken to keep the aspect ratio, expansion factor, and orthogonality angle in the desired range.

Figure 13 presents the conserved variables residues history in the simulation process for both mesh methods. It is important to mention that, in the case of the unstructured grid, the numerical procedure started oscillating around residues value of 1e–5. Therefore, a dissipative scheme is set up using a first-order discretization for the Navier–Stokes advection terms to avoid numerical instabilities, and then, after 100 iterations, the discretization order of advection terms in momentum equations was changed back to the second order.

Part II: Nonreacting Flow. The acoustic phenomenon in a gas turbine combustor can originate from different sources. Vibrating mechanical structures, regions of turbulent flow, and mixing of fluids with different temperatures are some examples for sound-generation mechanisms. However, earlier performed analyses on different types of noise sources in the combustor chamber showed that the acoustic noise induced by the unsteady combustion process is the strongest acoustic source [19]. This is of course missing in nonreacting calculations. To determine the exothermic effects on the flow in the model combustor, a nonreacting flow was first simulated as a reference by using different mesh types. The main parameters that were analyzed are pressure fluctuations, streamwise velocity, and also temperature in the case of hot flow. To observe the pressure fluctuations inside the combustion chamber, several locations along the length of the combustor are monitored, which are shown in Fig. 14. In this figure, P1–P6 represent the

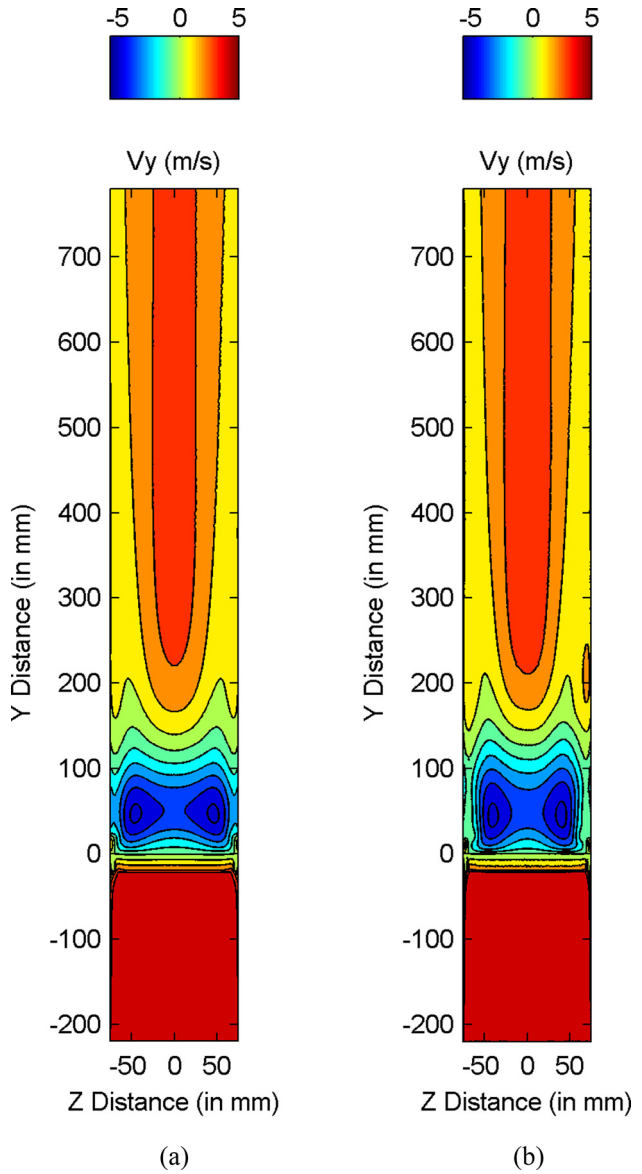

Fig. 9 Streamwise velocity component on the cross-sectional area B-B: (*a*) structured mesh; (*b*) unstructured mesh

location of both CFD monitor points and test rig pressure transducers, while T1–T4 stand for thermocouple locations.

Figure 15 shows the pressure spectra of the isothermal flows in the combustor with *nonreacting* mixture measured and calculated at three pressure transducer locations mounted downstream of the bluff body (numbers 4–6 in Fig. 14).

To have better visualization of the plots, the pressure data obtained from the *unstructured* grid has been *scaled down by a factor 5*. The combustor shows a self-excited acoustic mode at about 90 Hz. Other peaks of lower magnitude can be observed at multiple times the main frequency.

The comparison between the calculated and measured mean velocity on structured and unstructured meshes (Fig. 8) showed a minor dependence on the used mesh. The comparison of pressure data shows, however, an overprediction of a factor of 5 in the amplitude of oscillations by the unstructured mesh simulation in comparison with both measured data and structured mesh simulation data. In addition, the first mode calculated using the unstructured grid is underpredicted by 20 Hz. The higher harmonics are more damped and not so clear in this scheme.

The multimicrophone method is applied on the pressure data obtained from the CFD calculations (at the locations of pressure

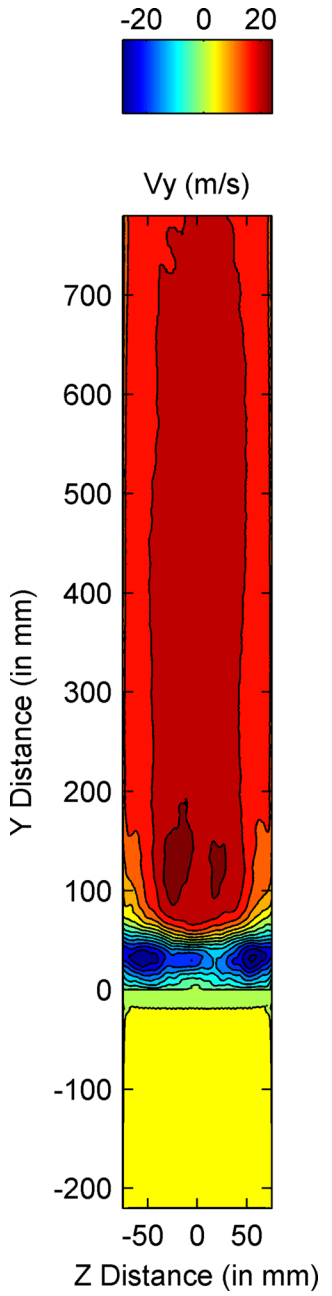

Fig. 10. Streamwise velocity component on the cross-sectional area B-B using BVM model power = 60 kW and $\lambda = 1.2$

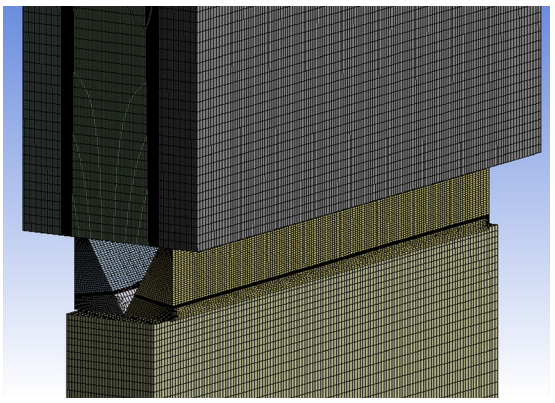

Fig. 11 Details of mesh around the bluff body for structured mesh

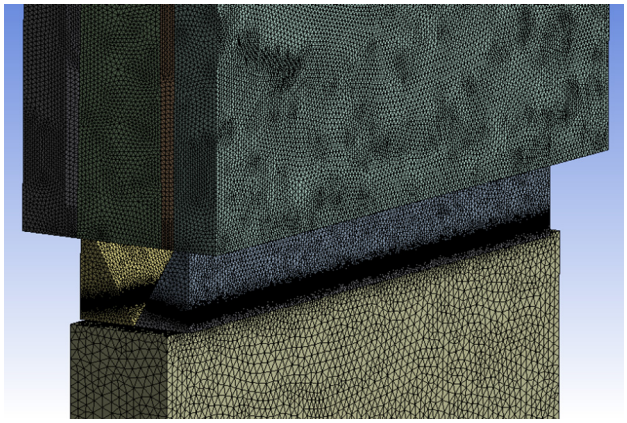

Fig. 12 Details of mesh around the bluff body for unstructured mesh

transducers P1–P6) to reconstruct the acoustic pressure and velocity fields.

Figure 16 shows the amplitude of pressure as well as velocity fluctuations measured at the first and the second peak frequencies against the height of the combustor. The origin of the axial axis in this case is taken at the center of the exit plane.

Therefore, zero in the x-axis corresponds to the exit of the burner, and the vertical thick line at −0.78 shows the position of the bluff body. The pressure antinode at the inlet and the node at the outlet of the combustor confirm that the open-closed acoustic boundary condition is established well by the numerical method. The pressure amplitude decreases along the combustor, and the maximum pressure occurs right above the bluff body, which matches the theoretical location of the maximum pressure for the first quarter wave. The pressure profile obtained at the second resonance peak (at about three times the first fundamental frequency) is consistent with the 3/4 wavelength resonant mode of an acoustic pipe.

Table 5 represents the values of reflection coefficients at the exit plane obtained from the simulation based on the structured grid and also from the experiment at the University of Twente for

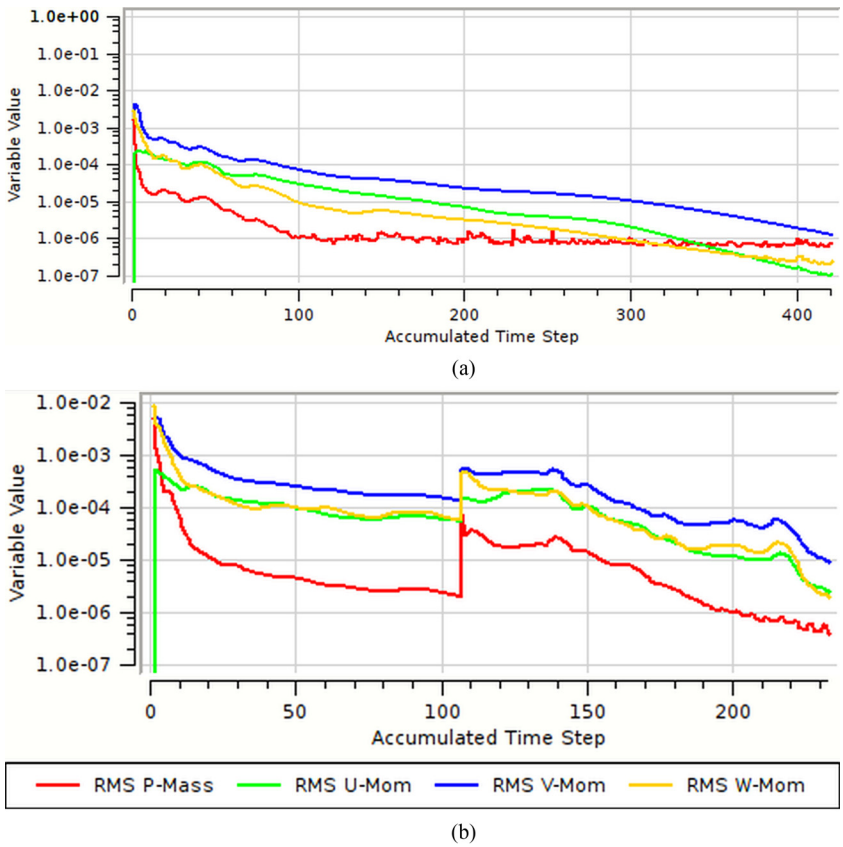

Fig. 13 Numerical residuals using structured (top) and unstructured mesh (bottom)

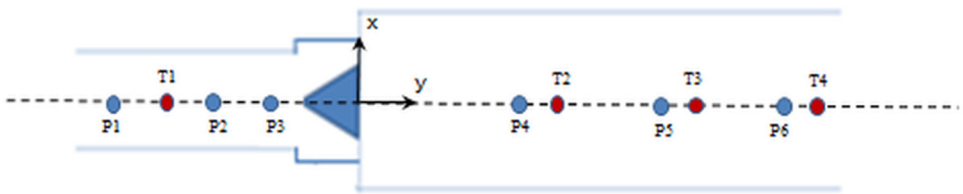

Fig. 14 Pressure and temperature monitoring points in the CFD domain: upstream and downstream of the wedge

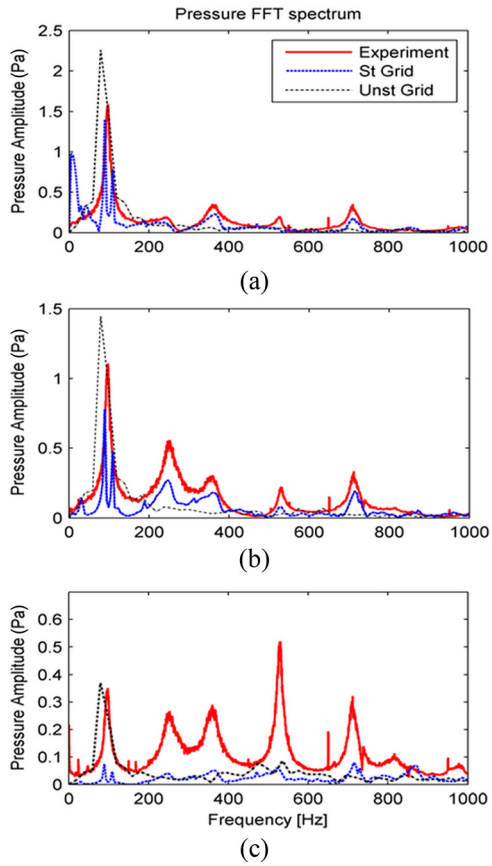

Fig. 15 FFT for 40 kW thermal power and air factor 1.4: experiment, structured mesh, unstructured mesh for different locations: (*a*) p4, (*b*) p5, (*c*) p6

the same operating condition. Quite good agreement can be seen between experiments and CFD data for the values of the reflection coefficients (R). These results prove that the combustor is acoustically open as R tends to unity.

Part III: Reacting Flow-Combustion Modeling Effect. The reacting premixed flow is studied experimentally and also with

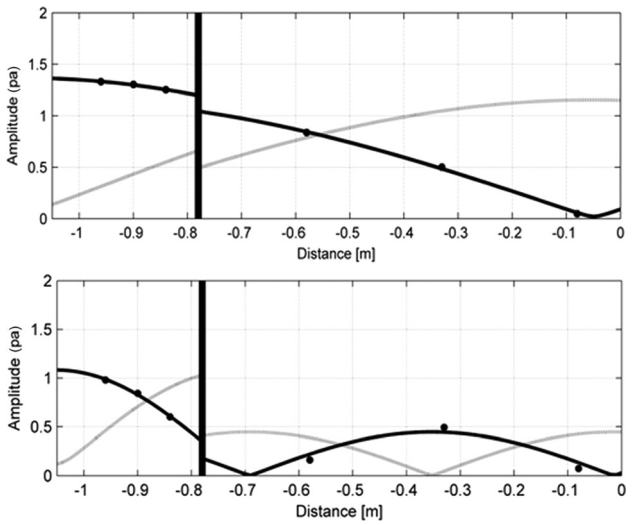

Fig. 16 Pressure (black line) and velocity (gray line) mode shape at the first fundamental frequency (top) and at the third quarter wave mode (bottom) for the structured grid calculations

Table 5 Reflection coefficients calculated at the exit of the combustor

CFD		Experiment	
|R|	Φ	|R|	Φ
0.98	−3.00	0.99	$-\pi$

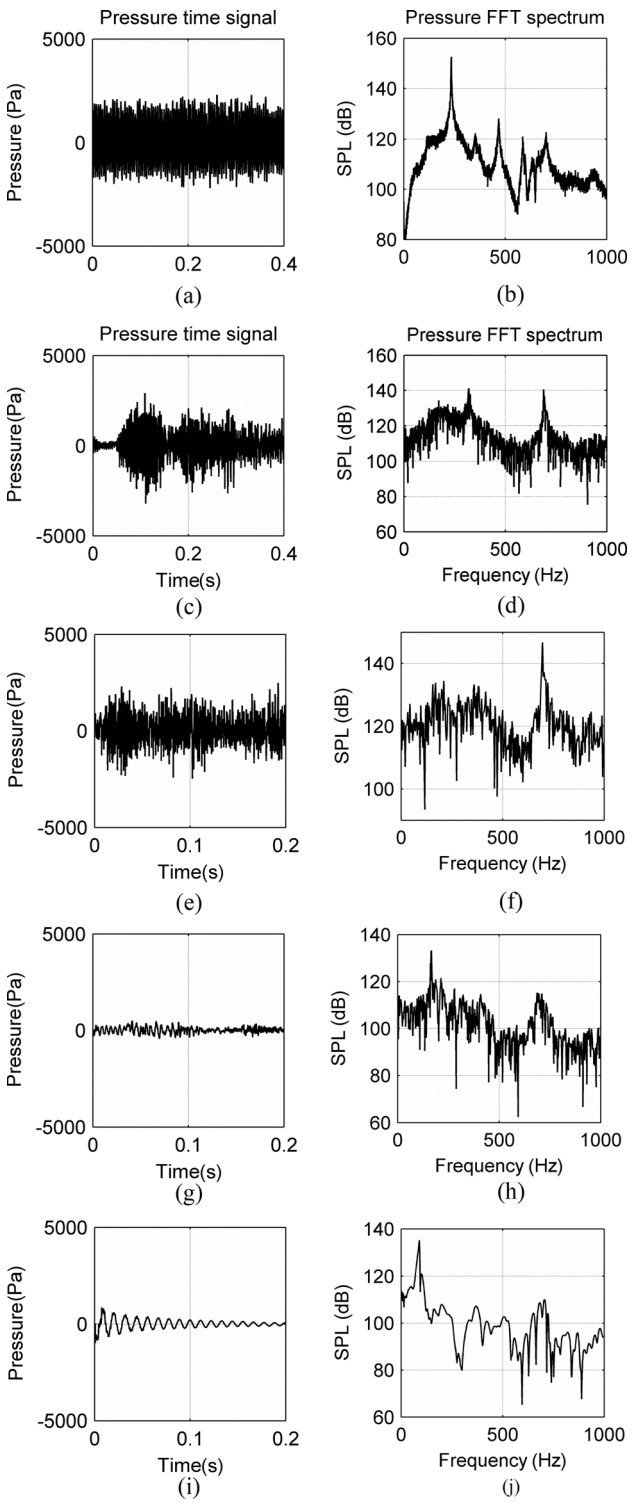

Fig. 17 Pressure fluctuations time history (left column) and FFT (right column) at power = 40 kW and $\lambda = 1.4$ measured at a location 200 mm downstream of the wedge from experiment ((*a*) and (*b*)), BVM ((*c*) and (*d*)), Pdf ((*e*) and (*f*)), EDM ((*g*) and (*h*)), and EDM-FRC ((*i*) and (*j*))

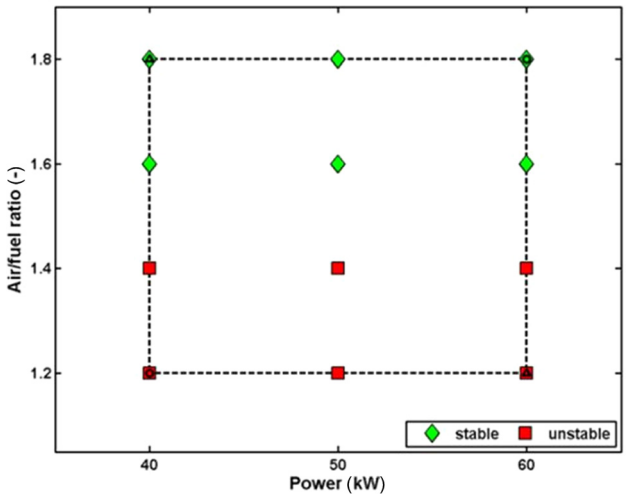

Fig. 18 Stability map of the LIMOUSINE combustor

four different combustion models. The reduced GRI MECH 3.0 was chosen as the detailed reference chemical reaction mechanism for these combustion models. Results are presented in Fig. 17 for air flow rate 19 g/s and a thermal power of 40 kW. For this flow, three clear self-excited modes are found experimentally at the University of Twente test rig, which are around 240 Hz, 480 Hz, and 720 Hz. To identify the nature of these modes, a finite element method (FEM) analysis has been done with the average temperature field given by the experimental data to obtain the acoustic eigenmodes. As Heckl [20] proposed, due to the area blockage of the burner, it can be assumed that the upstream and the downstream part of the combustor are acoustically decoupled; therefore, only the downstream duct has been taken into account in the FEM calculation. The obtained results confirm that the first and the third frequencies observed in the experiment are the first two acoustic modes of the combustor. The measured pressure signal shows limit cycle behavior with strong nonlinearities with a peak at twice the fundamental frequency [21]. Besides these modes, there are more peaks observed experimentally, which correspond to vibrational eigenfrequencies of the liner presented in Ref. [22]. Pressure fluctuation time history and fast Fourier transform (FFT) as obtained from simulations using different combustion models (all available in ANSYS-CFX) are presented in Fig. 17. Failure of the eddy dissipation/finite rate chemistry model can be concluded on the basis of its prediction of a stable flame (which is not the case for the investigated operating condition).

The probability density function (Pdf) flamelet model in CFX is originally designed for modeling of nonpremixed flames. Although testing this model for the LIMOUSINE combustor shows the model is able to predict the instability correctly, it failed in prediction of self-excited modes. The burning velocity model (BVM) is found to overpredict mean temperature and the rate of conversion to product species. The predicted temperature profiles are consistent with the overprediction of the molar fraction of major product species.

Fourier analysis of the pressure signal obtained from the BVM model yields two distinct peaks appearing at frequencies of about 319 and 638 Hz. Among the combustion models tested in this paper, that is the only model able to predict the frequency doubling of the first self-excited mode. These peaks were present in the experiment but with different amplitude and frequencies. Since in this paper, the mutual interaction between flow and the vibrating liner (due to the high-amplitude thermoacoustic instabilities) for the numerical computations has been neglected, the effect of the vibrating walls on the combustible flow is only visible in the experimental data. Numerical simulation by using LES at Centre Européen de Recherche et de Formation Avancée en Calcul Scientifique in the current combustor also predicted a dominant peak at 305 Hz and also the secondary peak 617 Hz (see Ref. [23]), which is close to the value calculated by the BVM model. Although there are some discrepancies between numerics and experiment in the prediction of fundamental frequency in this bluff body–stabilized combustor, the use of the BVM model for other applications on a swirl-stabilized flame computations shows promising results compared to the experimental data [24].

Conclusion and Future Work

In the paper, two structured-unstructured grid techniques in a finite volume method are used to simulate reacting and nonreacting flow in a partially premixed bluff body–stabilized model combustor. This paper has presented the performance of the combustion model for reacting configuration, and the main issues of the performed combustion modeling were reviewed. The following conclusions can be drawn from the present study:

- The obtained velocity fields resolved under structured and unstructured mesh conditions show minor dependence on the used mesh in the mean velocity compared to the PIV data, while the pressure fluctuations were found to depend heavily on the investigated grids.
- The unstructured mesh showed larger rates of mixing as compared to the structured mesh, and hence, this hints at significant numerical diffusion caused by the unstructured mesh discretization.
- Using the eddy dissipation/finite rate chemistry combustion model results in an unphysical stable flame (also flashback was observed). Although the Pdf flamelet model is able to predict the instability within the investigated combustion system, it failed in prediction of the frequency of the self-excited modes.
- The burning velocity model (BVM) is found to overpredict the mean temperature and rate of conversion to product species. However, this model is able to predict the frequency doubling of the first self-excited mode. To overcome the former problem, it is important to improve the boundary condition imposed to the liner. Of significance may be the influence of the prescribed liner boundary condition on the predictions. This influence is likely to be larger than in the stable combustion processes. In order to assess the energy transfer from the combustor to the ambient, besides considering the convection from the liner, heat transfer due to radiation (emission) from the quartz glass windows should be also taken into account.

Our future research targets the improvement of combustion modeling by using the CFI model linked to ANSYS (in-house code developed at University of Twente). The CFI model is a reaction progress variable model coupled to a reduced chemistry database.

Acknowledgment

The authors would like to acknowledge the funding of this research by the EC in the Marie Curie Actions Networks for Initial Training under call FP7-PEOPLE-2007-1-1-ITN, Project LIMOUSINE with project number 214905. Special thanks go to Dr. Phil Stopford for the support in the use of ANSYS-CFX.

Nomenclature

BVM = burning velocity model
EDM = eddy dissipation model
FFT = fast Fourier transform
FRC = finite rate chemistry model
P = pressure
T = temperature
v = streamwise velocity
λ = air excess ratio
Φ = phase of the signal (radian)

Appendix A

Limit Cycles of Thermoacoustic Oscillations in Gas Turbine Combustors. LIMOUSINE is a Marie Curie Initial Training Network funded by the European Commission under Framework 7. It represents a multidisciplinary initiative to strengthen the fundamental scientific work in the field of thermoacoustic instabilities in combustion systems and is motivated by the need for lean combustion technologies and reduced emissions. The research in LIMOUSINE is focused on the limit cycle behavior of the unstable pressure oscillations in gas turbines and on the resulting mechanical vibrations and materials fatigue.

Thermoacoustic instability can be caused by the feedback mechanism between unsteady heat release, acoustic oscillations, and flow perturbations. In a gas turbine combustor limit cycles of pressure oscillations at elevated temperatures generated by the unstable combustion process enhance the structural vibration levels of the combustor.

The LIMOUSINE combustor represents self-exited oscillations of high amplitude. Depending on the operating conditions (thermal power and air/fuel ratio), the flame shows a stable or an unstable behavior. Figure 18 shows the stability map of the combustor [22].

The self-excitation of combustion instabilities is linked to the phase relationship between the acoustic pressure field and unsteady heat release via Rayleigh's criterion [25]. The Rayleigh criterion, which recognizes the difference between damped or amplified interaction between pressure and heat release, is often used to investigate and predict combustion instabilities. It states that, if pressure and heat-release fluctuations are in phase, the instabilities are enhanced, whereas the instabilities are damped when the pressure oscillations and heat release are out of phase. This criterion is expressed as the following equation:

$$\iiint_{\Omega} p'q' \quad d\Omega > 0$$

where p' and q' are pressure and heat-release fluctuations, respectively, integrated over one cycle of the oscillation and Ω is the flow domain. Note that the integrals are also spatial, which means that both effects, destabilizing and stabilizing, can occur in different locations of the combustor and at different times, so the stability of the combustor will be decided by the net mechanical energy added to the combustor domain. Indeed, when the acoustic energy losses match the energy gain, stationary oscillatory behavior is obtained, which is referred to as the limit cycle oscillation [26].

Appendix B

Modeling of the Combustion. *Eddy Dissipation Model (EDM).* The eddy dissipation model [27] is based on the concept that chemical reaction is fast relative to the transport process in the flow. When reactants mix at the molecular level, they instantaneously form products. The model assumes that the reaction rate may be related directly to the time required to mix reactants at the molecular level.

By default, for the eddy dissipation model, it is sufficient that fuel and oxidant be available in the control volume for combustion to occur.

Combined EDM/Finite Rate Chemistry Model. For the combined finite rate chemistry/eddy dissipation model [27], the reaction rates are first computed for each model separately and then the minimum of the two is used. This procedure is applied for each reaction step separately, so while the rate for one step may be limited by the chemical kinetics, some other step might be limited by turbulent mixing at the same time and physical location.

Use of this model is recommended if reaction rates are limited by turbulent mixing in one area of the domain and limited by kinetics somewhere else.

Pdf Flamelet Model. The flamelet concept [28] for nonpremixed combustion describes the interaction of chemistry with turbulence in the limit of fast reactions (large Damköhler number). The combustion is assumed to occur in thin sheets with inner structures called flamelets. The turbulent flame itself is treated as an ensemble of laminar flamelets that are embedded into the flow field. The main advantage of the flamelet model is that, even though detailed information of molecular transport processes and elementary kinetic reactions is included, the numerical resolution of small length and time scales is not necessary. This avoids the well-known problems of solving highly nonlinear kinetics in fluctuating flow fields and makes the method very robust. Only two scalar equations have to be solved, independent of the number of chemical species involved in the simulation. Information of laminar model flames are precalculated and stored in a library to reduce computational time. On the other hand, the model is still restricted by assumptions like fast chemistry or the neglecting of different Lewis numbers of the chemical species.

The following list outlines the assumptions made to derive the flamelet model:

- fast chemistry
- unity Lewis numbers for all species ($Le = 1$)
- combustion is in the flamelet regime
- two feed system (i.e., fluid composition at boundaries must be pure "fuel," pure "oxidizer," or a linear blend of them)

Burning Velocity Model. In premixed and partially premixed flames, the flamelets have a discontinuity between the burnt and the unburnt regions; therefore, the model for premixed or partially premixed combustion can be split into two independent parts:

- model for the progress of the global reaction: burning velocity model (BVM), also called turbulent flame closure [27]
- model for the composition of the reacted and nonreacted fractions of the fluid: laminar flamelet with Pdf

In this model, a scalar (reaction progress) subdivides the flow field in two different areas: the burnt and the unburnt mixture. Burnt regions are treated similar to a diffusion flame, whereas the unburnt region is represented by the cold mixture. The mass fractions in the nonreacted fraction of the fluid, $Y_{i,fresh}$, are obtained by linear blending of fuel and oxidizer compositions. The species mass fractions in the burned fraction of the fluid, $Y_{i,burned}$, are computed by applying the flamelet model.

References

[1] Weatherill, N. P., 1988, "A Method for Generating Irregular Computational Grids in Multiply Connected Planar Domains," Int. J. Numer. Methods Fluids, **8**(2), pp. 181–197.

[2] Koomullil, R., Soni, B., and Singh, R., 2008, "A Comprehensive Generalized Mesh System for CFD Applications," Math. Comput. Simul., **78**(5–6), pp. 605–617.

[3] Mavriplis, D. J., 1997, "Unstructured Grid Techniques," Ann. Rev. Fluid Mech., **29**, pp. 473–514.

[4] Kikuchi, N., 1986, "Adaptive Grid-Design Methods for Finite Element Analysis," Comput. Methods Appl. Mech. Eng., **55**(1–2). pp. 129–160.

[5] Beam, R. M., and Warming, R., 1982, "Implicit Numerical Method for the Compressible Navier–Stokes and Euler Equations," lecture notes, Von Karman Institute for Fluid Dynamics, Sint-Genesius-Rode, Belgium.

[6] Caughey, D. A., and Hafez, M. M., 1994, *Frontiers of Computational Fluid Dynamics*, Wiley, New York.

[7] Çete, A. R., Yükselen, M. A., and Kaynak, Ü., 2008, "A Unifying Grid Approach for Solving Potential Flows Applicable to Structured and Unstructured Grid Configurations," Comput. Fluids, **37**(1), pp. 35–50.

[8] Hansen, R. P., and Forsythe, J. R., 2003, "A Comparison of Structured and Unstructured Grid Solutions for Flow Over a Circular Cylinder," Proceedings of the 2003 DoD User Group Conference, Bellevue, WA, June 9–13, pp. 104–112.

[9] Hua, Z.-L., Xing, L.-H., and Gu, L., 2008, "Application of a Modified Quick Scheme to Depth-Averaged κ–ε Turbulence Model Based on Unstructured Grids," J. Hydrodynam., **20**(4), pp. 514–523.

[10] Tomita, J. T., Silva, L. M. D., and Silva, D. T. D., 2012, "Comparison Between Unstructured and Structured Meshes With Different Turbulence Models for a High Pressure Turbine Application," Proceedings of ASME Turbo Expo, Copenhagen, Denmark, June 11–15, ASME Paper No. GT2012-69990.
[11] Rijke, P. L., 1859, "On the Vibration of the Air in a Tube Open at Both Ends," Philos. Mag., **17**, pp. 419–422.
[12] Patankar, S. V., 1980, *Numerical Heat Transfer and Fluid Flow*, Hemisphere, New York.
[13] Rhie, C. M., and Chow, W. L., 1982, "A Numerical Study of Turbulent Flow Past an Isolated Airfoil With the Trailing Edge Separation," AIAA J., **21**, pp. 1525–1532.
[14] Majumdar, S., 1988, "Role of Underrelaxation in Momentum Interpolation for Calculation of Flow With Nonstaggered Grids," Numer. Heat Transfer, **13**(1), pp. 125–132.
[15] Menter, F. R., 1994, "2-Equation Eddy-Viscosity Turbulence Models for Engineering Applications," AIAA J., **32**(8), pp. 1598–1605.
[16] Menter, F. R. and Egorov, Y., 2010, "The Scale-Adaptive Simulation Method for Unsteady Turbulent Flow Predictions. Part 1: Theory and Model Description," Flow Turbul. Combust., **85**(1), pp. 113–138.
[17] Combest, D. P., Ramachandran, P. A., and Dudukovic, M. P. 2011, "On the Gradient Diffusion Hypothesis and Passive Scalar Transport in Turbulent Flows," Ind. Eng. Chem. Res., **50**(15), pp. 8817–8823.
[18] Liu, M., 2012, "Age Distribution in the Kenics Static Micromixer With Convection and Diffusion," Ind. Eng. Chem. Res., **51**(20), pp. 7081–7094.
[19] Pozarlik, A., 2010, *Vibro-Acoustical Instabilities Induced by Combustion Dynamics in Gas Turbine Combustors*, University of Twente, Enschede, Netherlands.
[20] Heckl, M., 2010, "The Rijke Tube: A Green's Function Approach in the Frequency Domain," Acta Acust. Acust., **96**(4), pp. 743–752.
[21] Roman Casado, J. C., and Kok, J. B. W., 2012, "Non-Linear Effects in a Lean Partially Premixed Combustor During Limit Cycle Operation," Proceeding of ASME Turbo Expo 2012, Copenhagen, Denmark, June 11–15, ASME Paper No. GT2012-69164.
[22] Altunlu, A. C., Shahi, M., Pozarlik, A. K., van der Hoogt, P. J. M., Kok, J. B. W., and de Boer, A., 2012, "Fluid-Structure Interaction on the Combustion Instability," 19th International Congress on Sound and Vibration (ICSV19), Vilnius, Lithuania, July 8–12.
[23] Vera, I. H., 2011, "Soot Modeling in Flames and Large-Eddy Simulations of Thermo-Acoustic Instabilities," Ph.D. thesis, Universite de Toulouse, Toulouse, France.
[24] Ozcan, E., 2012, "Tuning the Self-Excited Thermo-Acoustic Oscillations of a Gas Turbine Combustor to Limit Cycle Operations by Means of Numerical Analysis," Master's thesis, University of Twente, Enschede, Netherlands.
[25] Rayleigh, J., 1878, "The Explanation of Certain Acoustic Phenomena," Nature, **18**, pp. 319–321.
[26] Shahi, M., Kok, J. B. W., and Alemela, P. R., 2012, "Simulation of 2-Way Fluid Structure Interaction in a 3D Model Combustor," Proceedings of ASME Turbo Expo, Copenhagen, Denmark, June 11–15, ASME Paper No. GT2012-69681.
[27] Ansys, 2010, Release 11.0 Documentation for ANSYS, Ansys Inc., Canonsburg, PA.
[28] Veynante, D., and Vervisch, L., 2002, "Turbulent Combustion Modeling," Prog. Energy Combust. Sci, **28**, pp. 193–266.